Supporting Information

Ultra-high Rate Li-S Batteries Based on Novel Conductive Ni_2P Yolk-shell Material as the Hosts for the S Cathode

Junhan Cheng; Dan Zhao; Lishuang Fan; Xian Wu; Maoxu Wang; Naiqing Zhang*; Kening Sun*.

Experimental Section

Materials: $Ni(NO_3)_2 \cdot 6H_2O$ was purchased from Aladdin Ltd (Shanghai, China). Glycerol, isopropanol were bought from Kermel Chemical Corporation (Tianjin, China). Ethanol was purchased from the Tianjin Chemical Corporation. All chemicals were used as received without further purification. The water use throughout all experiments was purified through a Millipore system (18.25 MΩ).

Synthesis of Ni_2P-YS and NiO-YS: In a typical synthesis of Ni-glycerate yolk-shell nanospheres, 1 mmol of $Ni(NO_3)_2 \cdot 6H_2O$ and 15 mL of glycerol were added into a 150 mL Teflon container pre-filled with 105 mL of isopropanol. After stirring for 5 min, 2 mL of deionized (DI) water was added into the above solution. After stirring for another 10 min, the container was then transferred to a stainless steel autoclave and kept in an electrical oven at 200 °C for 3-12 h. After cooling to room temperature naturally, the precipitate was separated by centrifugation, washed several times with ethanol and dried in an oven at 70 °C overnight. To obtain the Ni_2P yolk-shell nanospheres, the as-obtained Ni-glycerate yolk-shell precursor was then annealed at 300 °C in PH_3/Ar gas

flow for 2 h. The NiO yolk-shell nanospheres were prepared by the same annealed process in pure Ar atmosphere.

Synthesis of S@Ni_2P-YS and S@NiO-YS: The as-prepared Ni_2P-YS, NiO-YS and sulfur were ground together, heated to 155 °C in a sealed vacuum tube, and keep there for 24 h to facilitate sulfur diffusion into the Ni_2P, NiO host. Then, the composite was heated to 200 °C in a stabilized Ar atmosphere for 30min to clean the sulfur deposited on its outside surface.

Absorption of lithium polysulfides: Lithium polysulfide (Li_2S_6) was prepared according to the literature.[1] Typically, the stoichiometric amounts of sulfur (S) and lithium sulfide (Li_2S) with a molar ratio of 5:1 were dissolved in DOL:DME solvent by being magnetically stirred at room temperature under an argon atmosphere, yielding a yellow solution. The adsorption ability of the Ni_2P-YS on lithium polysulfide was investigated by UV-vis spectroscopy. Typically, 20 mg of Ni_2P-YS and NiO-YS was placed in 3 mL of Li_2S_6 solution (10 $mmol \cdot L^{-1}$), and the mixture was stirred for 2 h. The suspensions were centrifuged before photographs and UV-vis test.

Characterization: The morphologies of the samples were confirmed by field-emission scanning electron microscopy (FE-SEM, Hitachi SU8010,15kV) and transmission electron microscopy (TEM, Tecnai G2 F30, 200kV). The phase analysis datum were collected by powder X-ray diffraction technology, using a X-ray diffractometer (Panalytical X'pert pro) with Cu Kα X-ray radiation (λ=1.5418 Å). The nitrogen sorption isotherm was measured with a Micromeritics ASAP 2020 adsorption analyser at 77 K. Before the measurements, the samples were degassed at 150 °C for 6 h. Thermogravimetric analyses (TGA) was conducted on a thermogravimetric analyser

(Linseis STA PT 1600) under stable N_2 flow with a heating rate of 10 $^oC \cdot min^{-1}$. The adsorption performance of lithium polysulfide was measured using a UV-vis spectrophotometer (Kyoto UV-2450). X-ray photoelectron spectroscopy (XPS) analysis was performed at room temperature to analyze the electrode and contents of element. The electronic conductivity was characterized at room temperature with a four-probe conductivity test meter (Jandel RM300). Before test, the material has been compressed under 20MPa to form a thick flake.

Electrochemical measurement: All the electrochemical tests require a coin-type half-cell (CR 2025). Before assemble the test cell, the as-prepared S@Ni_2P-YS sample was mixed with Super_P and polyvinylidene fluoride (PVDF) at a weight ratio of 8:1:1 in N-methyl-2-pyrrolidone (NMP) solution to form homogeneous slurry, which was then pasted on Al foil and dried in a vacuum over at 60 °C for 12 h to remove the solvent and moisture totally. The bare Ni_2P electrodes without sulfur loaded are prepared under the same condition. Test cells were assembled with the S@Ni_2P-YS as the working electrode, the metallic lithium foil as the counter electrode, 1 $mol \cdot L^{-1}$ lithium bis(trifluoromethanesulfone)imide (LiTFSI) in 1,3-dioxolane (DOL) and dimethoxymethane (DME) (1:1 in volume) as the electrolyte with 2 wt% $LiNO_3$ as an additive, and a trilayer polypropylene-polyethylene-polypropylene (PP/PE/PP) membrane (Celgard 2300) as the separator. All the operation was executed in a glovebox under pure Argon-filled atmosphere with moisture and oxygen partial pressure under 1 ppm. Cyclic voltammetry (CV) were carried out on a CHI 710E electrochemical workstation (CH Instruments, Inc., Shanghai) in the potential range of 1.8-2.8 V (vs. Li/Li^+) at a different scanning rate. The electrochemical impedance

spectroscopy (EIS) was carried out with a PARSTAT 2273 (Princeton Applied Research, USA) electrochemical system over a frequency range from 1 MHz to 1 Hz. The galvanostatic charge-discharge tests were conducted on a Neware battery-testing system (5 V, 5 mA & 50 mA) based on different current density of the working electrode.

Result and discussion

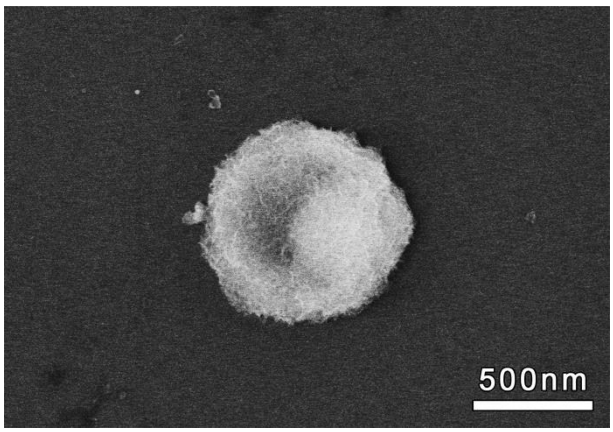

Figure S1. High magnification SEM image of Ni-YS precursor.

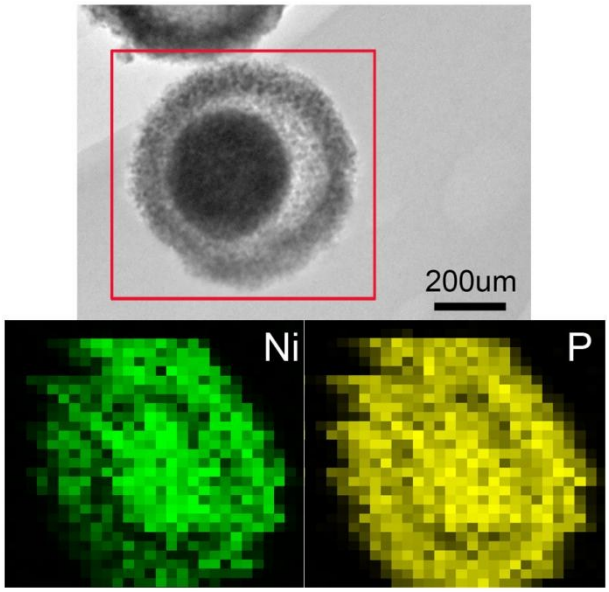

Figure S2. The EDX elemental mappings of nickel and phosphorus.

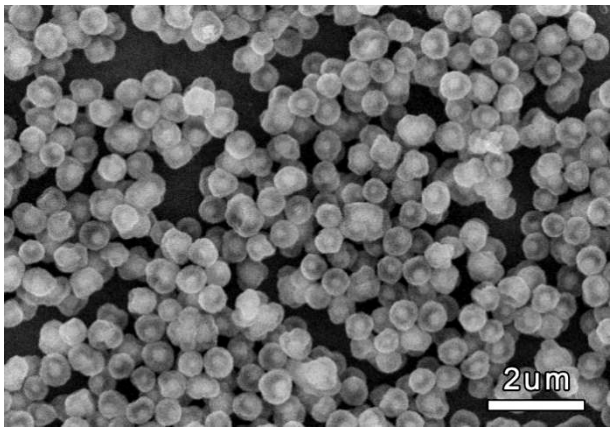

Figure S3. SEM image of the NiO-YS

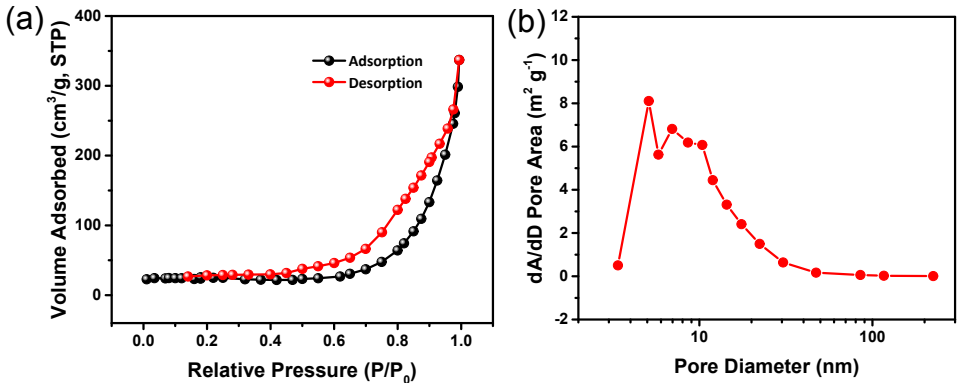

Figure S4. (a) N_2 sorption isotherm and the (b) pore size distribution of NiO-YS.

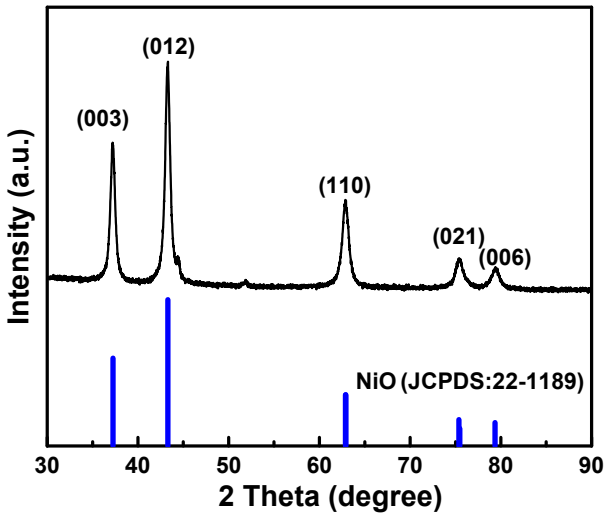

Figure S5. XRD pattern of NiO-YS and corresponding standard card.

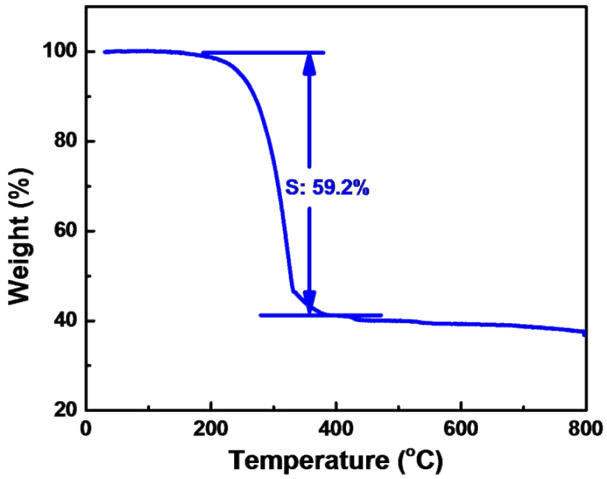

Figure S6. TGA curves of sulfur and S@NiO-YS in N_2 flow.

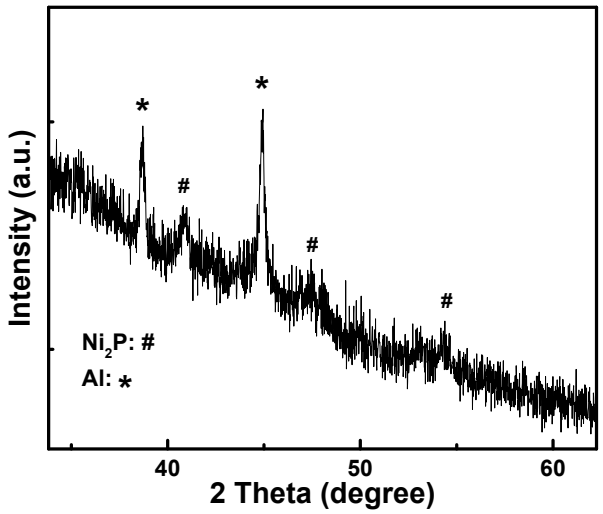

Figure S7. XRD pattern of S@Ni_2P-YS after 100 cycles.

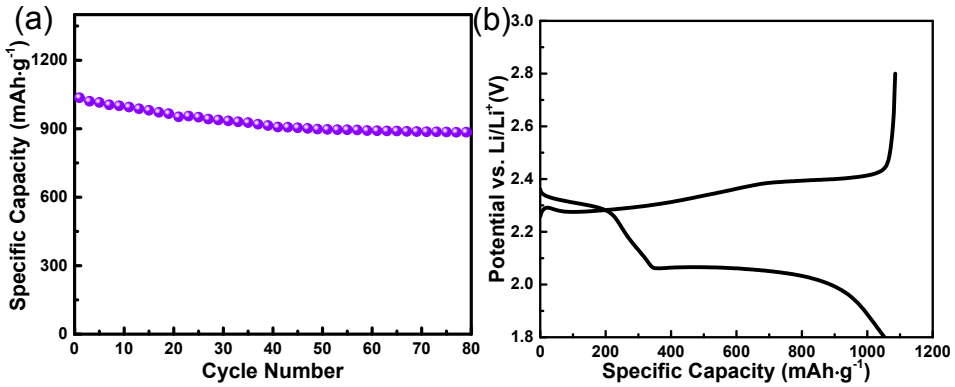

Figure S8. (a) Cycling performance of S@NiO-YS over 80 cycles and (b) Galvanostatic charge/discharge profiles of S@NiO-YS at a charge/discharge rate of 0.2C.

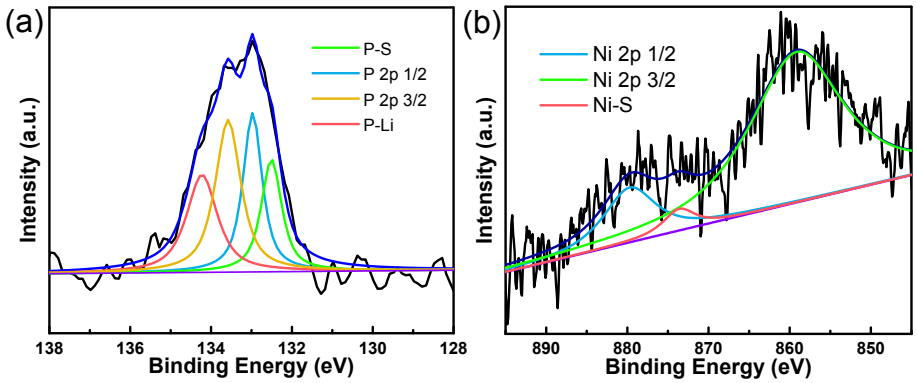

Figure S9. XPS spectra of (a) P 2p and (b) Ni 2p for the electrode after 100 cycles.

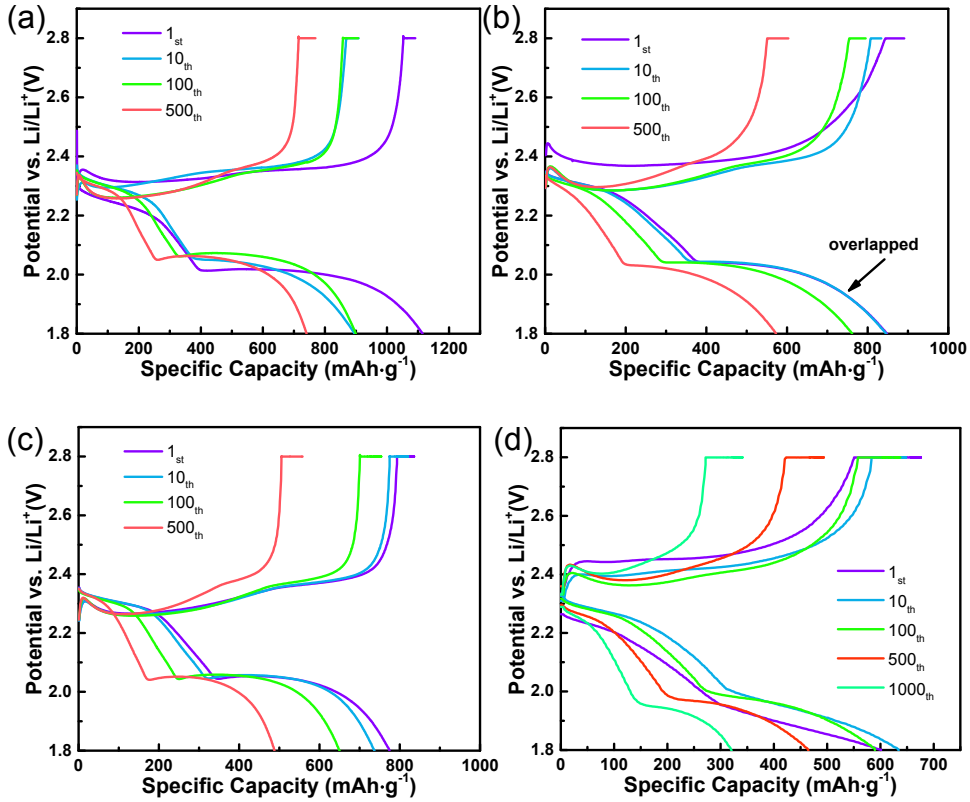

Figure S10 Galvanostatic charge/discharge profiles during cycling of S@Ni_2P-YS at (a) 1C, (b) 2C, (c) 3C and (d) 5C.

Table S1. Parameters and cell performance of polar cathode material in Li-S batteries.

Cathode Materials	S content (wt%)	Cycle capacity ($mAh \cdot g^{-1}$)		Rate capacity ($mAh \cdot g^{-1}$)		Title	Ref.
		Initial	Retention	Initial	Retention		
S@$Co(OH)_2$	75	1014 (0.1C)	653 (100 cycles)	747 (0.5C)	491 (100 cycles)	Double-Shelled Nanocages with Cobalt Hydroxide Inner Shell and Layered Double Hydroxides Outer Shell as High-Efficiency Polysulfide Mediator for Lithium-Sulfur Batteries	[2]
S@PEDOT/MnO_2	87	1150 (0.2C)	827 (200 Cycles)	910 (0.5C) 685 (1C)	545 (200 cycles) 365 (200 cycles)	Manganese dioxide nanosheet functionalized sulfur@PEDOT core-shell nanospheres for advanced lithium-sulfur batteries†	[3]
Sulfur-TiO_2	71	1030 (0.5C)	690 (1000 cycles)	630 (2C)	N/A	Sulphur-TiO_2 yolk-shell nanoarchitecture with internal void space for long-cycle lithium-sulphur batteries	[4]
Droped TiO_2/S	68	1171 (0.5C)	820 (700 cycles)	N/A	N/A	Tailoring Surface Acidity of Metal Oxide for Better Polysulfide Entrapment in Li-S Batteries	[5]
Ti_nO_{2n-1}	64.2	1044 (0.1C).	99% (100 cycles)	527 (1C)	N/A	Strong Sulfur Binding with Conducting Magnéli-Phase Ti_nO_{2n-1} Nanomaterials for Improving Lithium–Sulfur Batteries	[6]
$Li_2S@MS_2$ M=Ti, Zr, V	72	1156 (0.2C)	86% (150 cycles)	956 (0.5C)	77% (400 cycles)	Two-dimensional layered transition metal disulphides for effective encapsulation of high-capacity lithium sulphide cathodes	[7]
MoO_2/S	38	1100 (0.1C)	570 (250 cycles)	545 (5C)	N/A	Strong Surface-Bound Sulfur in Conductive MoO_2 Matrix for Enhancing Li-S Battery Performance	[8]
TiC@G	61	1032 (0.2C)	670 (100 cycles)	N/A	N/A	Enhanced Electrochemical Kinetics on Conductive Polar Mediators for Lithium-Sulfur Batteries	[9]
S@a-NiS_2	63	1238 (0.5 $A \cdot g^{-1}$)	954 (1200 cycles)	800 (2 $A \cdot g^{-1}$)	N/A	High performance Li-S battery based on amorphous NiS- as the host material for the S cathode	[10]
MnO_2@S	85	1080 (0.5C)	950 (300 cycles)	900 (2C)	315 (1700 cycles)	In Situ Reactive Assembly of Scalable Core–Shell Sulfur–MnO_2 Composite Cathodes	[11]
S/VO_2-graphene	80	1180 (0.05C)	N/A	950 (0.5C)	≈400 (1000 cycles)	Tuning Transition Metal Oxide-Sulfur Interactions for Long Life Lithium Sulfur Batteries: The "Goldilocks" Principle	[12]
S/MnO_2	75	1300 (0.05C)	N/A	≈830 (2C)	245 (2000 cycles)	A highly efficient polysulfide mediator for lithium-sulfur batteries	[13]
MnO_2@HCF/S	71	1147 (0.2C)	≈900 (100 cycles)	≈900 (0.5C)	662 (300 cycles)	Hollow Carbon Nanofibers Filled with MnO_2 Nanosheets as Efficient Sulfur Hosts for Lithium-Sulfur Batteries	[14]
S@CB hybrids@thin $Ni(OH)_2$ layers	78.4	968 (0.2C)	1250 (500 cycles)	195 (5C)	N/A	Encapsulation of sulfur with thin-layered nickel-based hydroxides for long-cyclic lithium-sulfur cells	[15]
S@Ni_2P yolk-shell	65.1	1409 (0.2C)	919 (100 cycles)	924 (1C) 848 (2C) 714 (3C) 602 (5C) 439 (10C)	737 (500 cycles) 575 (500 cycles) 524 (500 cycles) 321(1000 cycles) N/A	This work	

Table S2. The electrochemical properties of S@Ni_2P-YS and S@NiO-YS electrodes toward polysulfide conversion reactions

	Peak Potential (V)			Peak Current Density ($A \cdot g^{-1}$)	
	Reduction (E_{pc})	Oxidation (E_{pa})		Reduction (I_{pc})	Oxidation (I_{pa})
S@Ni_2P-YS	**2.32, 2.05**	**2.29, 2.37**		**0.84, 1.82**	**2.26, 1.83**
S@NiO-YS	**2.31, 2.04**	**2.34, 2.39**		**0.72, 1.08**	**1.32, 1.42**

Table S3. The EIS simulation result of S@Ni_2P-YS and S@NiO-YS

	$R_u(\Omega)$	Q_{cd} (F)	$Q_{cd,n}$	R_{ct} (Ω)	Q_{zw} (Ω)	$Q_{zw,n}$
S@Ni_2P-YS	**4.46**	**3.84×10^{-5}**	**0.767**	**29.84**	**1.83×10^{-4}**	**0.976**
S@NiO-YS	**3.57**	**6.67×10^{-6}**	**0.853**	**125.1**	**4.65×10^{-4}**	**0.826**

Reference

1. Z. Yuan, H. J. Peng, T. Z. Hou, J. Q. Huang, C. M. Chen, D. W. Wang, X. B. Cheng, F. Wei and Q. Zhang, *Nano Lett*, 2016, **16**, 519-527.
2. J. Zhang, H. Hu, Z. Li and X. W. Lou, *Angewandte Chemie*, 2016, **55**, 3982-3986.
3. M. Yan, Y. Zhang, Y. Li, Y. Huo, Y. Yu, C. Wang, J. Jin, L. Chen, T. Hasan, B. Wang and B.-L. Su, *J. Mater. Chem. A*, 2016, **4**, 9403-9412.
4. Z. Wei Seh, W. Li, J. J. Cha, G. Zheng, Y. Yang, M. T. McDowell, P. C. Hsu and Y. Cui, *Nat Commun*, 2013, **4**, 1331.
5. X. Wang, T. Gao, X. Fan, F. Han, Y. Wu, Z. Zhang, J. Li and C. Wang, *Adv Funct Mater*, 2016.
6. X. Tao, J. Wang, Z. Ying, Q. Cai, G. Zheng, Y. Gan, H. Huang, Y. Xia, C. Liang, W. Zhang and Y. Cui, *Nano Lett*, 2014, **14**, 5288-5294.
7. Z. W. Seh, J. H. Yu, W. Li, P. C. Hsu, H. Wang, Y. Sun, H. Yao, Q. Zhang and Y. Cui, *Nat Commun*, 2014, **5**, 5017.
8. Q. Qu, T. Gao, H. Zheng, Y. Wang, X. Li, X. Li, J. Chen, Y. Han, J. Shao and H. Zheng, *Adv Mater Interfaces*, 2015, **2**, 1500048.
9. H. J. Peng, G. Zhang, X. Chen, Z. W. Zhang, W. T. Xu, J. Q. Huang and Q. Zhang, *Angewandte Chemie*, 2016.
10. Z. Liu, X. Zheng, S.-l. Luo, S.-q. Xu, N.-y. Yuan and J.-n. Ding, *J. Mater. Chem. A*, 2016, **4**, 13395-13399.
11. X. Liang and L. F. Nazar, *Acs Nano*, 2016, **10**, 4192-4198.
12. X. Liang, C. Y. Kwok, F. Lodi-Marzano, Q. Pang, M. Cuisinier, H. Huang, C. J. Hart, D. Houtarde, K. Kaup, H. Sommer, T. Brezesinski, J. Janek and L. F. Nazar, *Adv Energy Mater*, 2016, **6**, 1501636.
13. X. Liang, C. Hart, Q. Pang, A. Garsuch, T. Weiss and L. F. Nazar, *Nat Commun*, 2015, **6**, 5682.
14. Z. Li, J. Zhang and X. W. Lou, *Angewandte Chemie*, 2015, **54**, 12886-12890.
15. J. Jiang, J. Zhu, W. Ai, X. Wang, Y. Wang, C. Zou, W. Huang and T. Yu, *Nat Commun*, 2015, **6**, 8622.